Selective Lignin Depolymerization via Transfer Hydrogenolysis Using Hydrotalcite Supported Palladium – Model Compounds to Application

[a] Darren Dolan, [a] Rebekah Brucato, Adelina M. Voutchkova-Kostal[a*]

[a] Chemistry Department, the George Washington University, 800 22nd St NW, Washington D.C. 20910;

Novelty: (i) transfer hydrogenolysis of α-O-4, β-O-4 and 4-O-5 model compounds using ethanol as renewable hydrogen source; **(ii)** multifunctional catalyst for tandem transfer hydrogenolysis and decarbonylation of β-O-4 motifs; (iii) whole lignin valorization to phenolic derivatives using only ethanol as hydrogen donor

Abstract

The cleavage of lignin ether bonds via transfer hydrogenolysis remains a promising route for the valorization of lignin. To make this process efficient, a method would need to be developed that utilizes mild conditions and a renewable hydrogen donor solvent, in addition to avoiding high pressure of hydrogen. Herein, we demonstrate the efficient catalytic transfer hydrogenolysis of lignin model compounds possessing aromatic ether bonds, including α-O-4, β-O-4 and 4-O-5 linkages, using Pd-doped hydrotalcites as heterogeneous catalysts and ethanol as the hydrogen donor. Catalysts that can carry out transfer hydrogenolysis and decarbonylation in tandem are yet to be reported. Quantitative conversions and yields were realized for all model compounds studied, demonstrating the utility of the metal-doped hydrotalcites for this catalytic application. The system was applied to whole pine biomass to achieve delignification (86%) and a phenolic monomer yield of 39%.

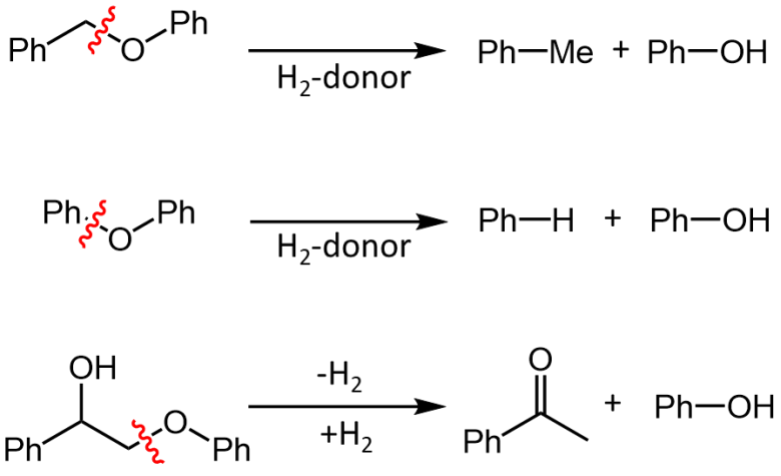

Introduction

The need to shift to platform chemicals derived from renewable and non-food competitive sources is emphasized in both the principles of green chemistry and the UN Sustainable Development goals (specifically goals 7, 9 and 11).[1] Lignin has received considerable interest as a bioderived chemical source due to its potential for high quality aromatic production through depolymerization and the fact that it is not competitive with food production.[2-4] Currently, >98% of lignin co-produced is incinerated for energy recovery, which does not capture its potential to provide more valuable chemical feedstocks. At such a large scale, selective, energy-efficient, and clean depolymerization to afford desirable compounds is needed to make this process economically viable.

The key challenge associated with lignin depolymerization is the asymmetric and branched nature of the polymer, composed of C-O bonds found in β-O-4, α-O-4, and 4-O-5 ether linkages.[5] These C-O linkages are dominate targeted functional group for depolymerization of native lignin due to their lower bond dissociation energies compared to C-C linkages. However, selective cleavage under relatively mild conditions is challenging. The majority of depolymerization methods rely on hydrogenolysis with exogenous hydrogen, most often derived from fossil fuel sources.[6-22] While alternative methods, such as oxidation[23-28], hydrolysis [29-35], hydrothermal [36-39], photo-[40, 41] and electro-chemical[42] transformations have also been extensively explored, transfer hydrogenolysis (TH) is particularly promising for selective depolymerization under relatively mild conditions under hydrogen-free conditions. TH conditions is advantageous for minimizing energy input and avoiding undesired hydrogenation of aromatic rings.

TH of lignin model compounds has been primarily performed with formic acid, formate salts and isopropyl alcohol as hydrogen donors – all of which are derived from non-renewable sources, as summarized in two recent reviews.[43] The ability to perform TH with ethanol as the hydrogen donor, and under relatively mild conditions, is highly advantageous. Ethanol has been widely accepted as a green solvent due to its availability from fermenting renewable sugars and

starches, its relatively low cost compared to alternative hydrogen donors, and its low hazard.[44, 45]

Table 1. Transfer hydrogenolysis of β-O-4 lignin model compounds over supported catalysts.

Substrate, conditions, products, yield	Conversion, %	Reference
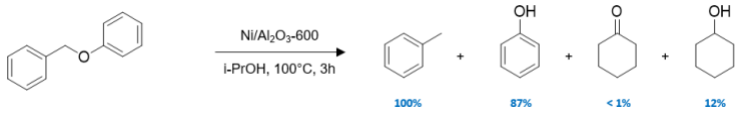	100	[46]
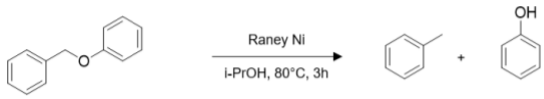	100	[47]
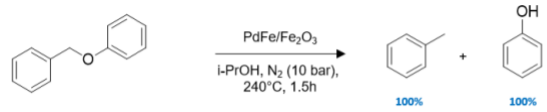	100	[48]
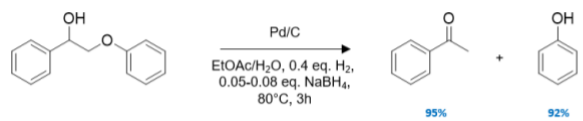	100	[49]
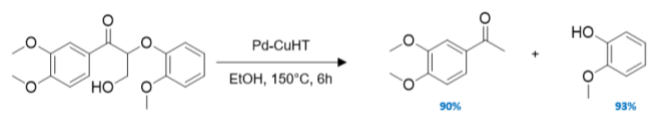	>98	This work

While catalytic transfer hydrogonolysis of lignin model compounds has been reported (Table 1), the tandem catalytic transfer hydrogenolysis *and* decarbonylation with the same catalyst in the same pot is yet to be reported. Optimizing the activity and selectivity of multifunctional catalysts capable of such tandem transformations is challenging since the steps can be interdependent. The latter requires control over the size, location, and structure of catalytically active species, and mechanistic insight into corresponding structure-activity relationships, including the role of supports.[50] Efforts by our group and others to develop Pd catalysts on active, tunable supports for organic synthesis and biomass valorization take advantage of cooperative

catalytic activity of the support and strong interactions with support matrices that regulate metal speciation, reactivity and stability.[51-57,58]

MgO and *γ*-Al_2O_3 supported metal catalysts are well-known to present divergent acid-base properties:[59-62] Saad et al. reported Pt-supported MgO displays strong basicity, whereas Pt-Al_2O_3 displays strong acidity.[58] Similar observations were made by Groppo et al. for Pd analogues.[63] Hydrotalcites (HTs) are a sub-set of LDHs with formula $[M^{2+}_{1-x}M^{3+}_{x}(OH)_2]^{x+}(A^{n-})_{x/n}.mH_2O$, where M^{2+} and M^{3+} are Mg^{2+}, Al^{3+} or compatible alkali earth and transition metal cations.[64] Although LDH materials similar to HT exhibit basic properties approaching those of MgO,[65] the tuneable nature of such materials means that both O^{2-} Lewis base and Al^{3+} Lewis acid centres are accessible.[66, 67]

The unique reactivity of Pd-doped LDH (or HT) catalysts includes decarbonylation of aldehydes,[53] aldol condensations[51] and acceptorless alcohol and amine dehydrogenation:[52, 68] elementary steps in deoxygenative olefination of alcohols. Recently, we reported Pd-HT catalysts are highly active for the atom-economical olefination of carbonyls via aldol-decarbonylative coupling, producing only CO and H_2O by-products[51] as well as the conversion of alcohols to long-chain hydrocarbons via initial acceptorless dehydrogenation of the alcohol.[69]

Here we demonstrate the feasibility of one-pot, hydrogen-free and base-free cleavage of α-O-4, β-O-4 and 4-0-5 linkers of lignin using multifunctional Pd catalysts, featuring supports possessing different acid-base properties:[70, 71] MgO, with primarily basic character; a HT with Lewis acidic and basic sites; and γ-Al_2O_3, with primarily acidic character. The cleavage consists of tandem dehydrogenation, hydrogenolysis and decarbonylation reactions – all facilitated by the same catalyst. The novelty of the present work is threefold: **(i)** transfer hydrogenolysis of α-O-4, β-O-4 and 4-O-5 model compounds using ethanol as renewable hydrogen source; **(ii)** multifunctional catalyst for tandem transfer hydrogenolysis and decarbonylation of β-O-4 motifs; and **(iii)** whole lignin valorization to phenolic derivatives using only ethanol as hydrogen donor.

Experimental Section

Materials and Chemicals

Aluminum (III) nitrate nonahydrate (98%) and magnesium (II) nitrate hexahydrate (98%) were obtained from ACROS Organics. Palladium (II) nitrate hydrate (40% palladium basis) and palladium (II) acetate (98%) were purchased from Sigma Aldrich. γ-Alumina (150 mesh, 58 Å) was purchased from Aldrich Chemical Company. Sodium hydroxide (97%) was obtained from VWR AMRESCO® Life Sciences and sodium carbonate (99.5%) from Fisher Scientific. Compounds used to synthesize model compounds including acetophenone (>98 %), 2-phenoxyacetophenone (>98 %), 3,4-dimethoxyacetophenone (>98%), phenol (>99%), and guaiacol (>98%) were obtained from TCI Chemicals. Formaldehyde solution (37 wt% in water) was acquired from Beantown Chemicals, sodium borohydride (99%, Venpure™ SF granules) was purchased from Acros Organics, and bromine (>98 %) was purchased from Aldrich Chemicals. Diphenyl ether (>98 %) and benzyl phenyl ether (>98 %) was purchased from TCI Chemicals and used without further purification.

Catalyst Preparation and Characterization

Pd-Al_2O_3 and Pd-MgO were synthesized via a wet impregnation method and Pd-HT was synthesized via a continuous flow precipitation from previously reported methods (see Supporting Information, SI, for details).[72, 73]

Inductively coupled plasma optical emission spectroscopy (ICP-OES) was employed to measure the metal content of the catalyst. Powder X-Ray Diffraction (PXRD) patterns were obtained to determine crystalline phases present in addition to crystalline parameters such as crystallite size and *d* spacing. X-ray photoelectron spectroscopy (XPS) was employed to determine metal speciation for any Pd species present. X-ray Photoelectron Spectroscopy (XPS) was utilized to determine palladium speciation within the catalysts. Transmission electron microscopy (TEM) was employed to determine the presence of Pd nanoparticles. Attenuated total reflection Fourier Transform-Infrared (ATR-FTIR) spectroscopy was employed to visualize vibrational modes that are characteristic of hydroxyl groups present on the catalysts surface of the cationic sheet and carbonate ions present in the catalysts inter layer. Nitrogen adsorption-desorption analysis was used to determine the surface area, pore size, and pore volume of the catalysts. Specific surface

area was calculated according to the Brunauer-Emmett-Teller (BET) theory, while pore sizes and volumes were determined according to the Barrett-Joyner-Halenda (BJH) model applied to desorption isotherms. Thermogravimetric analysis (TGA) was utilized to understand the thermal stability of the catalysts in addition to moisture loss.

Nuclear magnetic resonance and gas chromatography-mass spectrometry was implemented for the qualitative determination of unknown product mixtures. Quantitative analyses were carried out via gas chromatography-flame ionization detection.

Model Compound Reactions

Reactions were carried out under microwave conditions using an Anton Parr Monowave 450. Lignin model compounds (Figure 1) (0.1 mmol) were placed in a G10 Anton Parr glass microwave vial with a magnetic stir bar. Solvent (3.0 mL) and catalyst (5.0 mol % Pd) was added and agitated for dispersion. The vial was sealed, placed in the microwave system, and carried out for the specified time and temperature with a stir rate of 600 rpm. The catalyst was separated by filtration after the reaction. Gas chromatography-mass spectrometry (GC-MS) was used to identify the chemicals in the product mixture. Products were then quantitatively analyzed via gas chromatography – flame ionization detection (GC-FID)

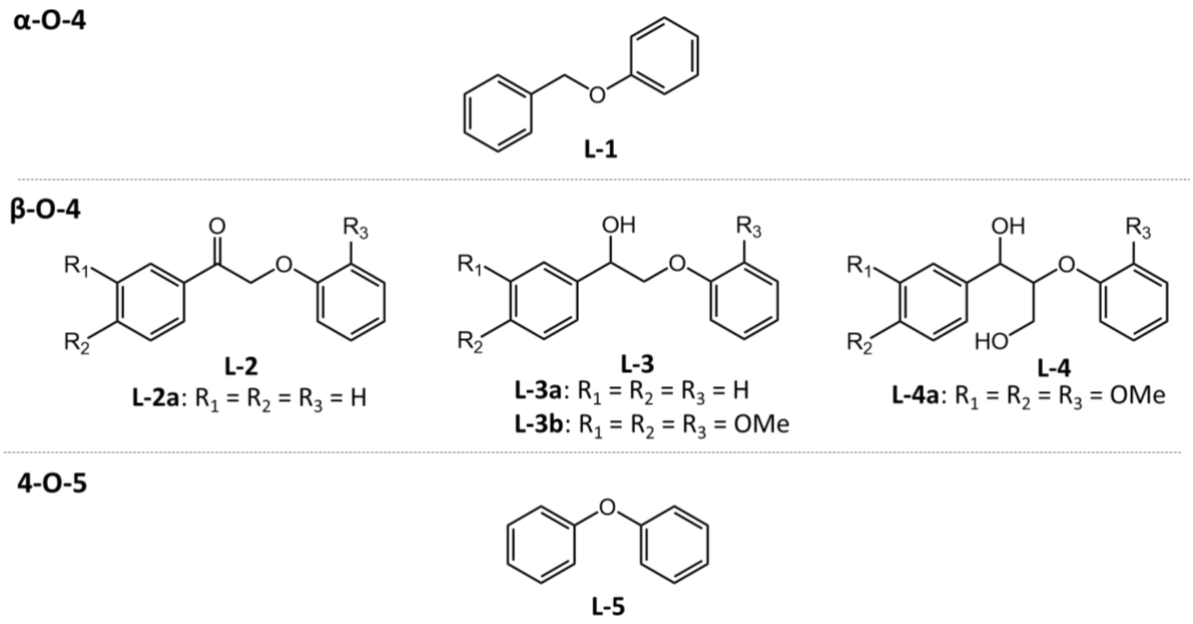

Figure 1. Lignin motifs examined via model compounds L-**1** through L-**5**.

Whole Pine Reductive Catalytic Fractioning (RCF)

Pine sawdust (5.0 g), ethanol (50 mL), and 5% Pd-HT (0.60 g) were loaded in a 100 mL borosilicate liner in a Parr autoclave reactor. The reactor was sealed, stirring started, and allowed to come to temperature (200-225 °C) before starting the reaction time (3 h). Upon completion, the reaction was allowed to cool to 50 °C before filtering. The residual pulp was washed with ethanol (3 x 20 mL), acetone (3 x 20 mL), and water (20 mL). The filtrate was concentrated in *vacuo* and the crude product mass was determined. The filtered cellulose pulp residue was dried under vacuum overnight at 70 °C and weighed. Lignin and small molecules were extracted from the crude product using ethyl acetate (3 x 150 mL) and sonication for 20 minutes after each addition. The ethyl acetate layers were combined and filtered over celite before removing the solvent in *vacuo*. The lignin oil was weighed, and yield was determined. The lignin oil was subsequently characterized by ^{1}H-NMR and GC-MS to analyze monomer formation. A detailed explanation for the determination of the following can be found in Supporting Information: (i) biomass moisture content, (ii) lignin content of the biomass, (iii) lignin yield, and (iv) monomer yield.

Results and Discussion

Pd-γ-Al_2O_3, Pd-MgO, and a multitude of Pd-*x*HT's (*x* = transition metal dopant) were synthesized and characterized with the goals of (i) assessing their activity for the transfer hydrogenolysis of common lignin ether linkages to afford valuable phenolic platform chemicals; and (ii) identifying the physical and chemical features of each catalyst that are responsible for higher catalytic activity and selectivity to desired products. Pd loading was targeted at 2-5 wt% for Pd-γ-Al_2O_3, Pd-MgO, and Pd-HT. Pd-γ-Al_2O_3 and Pd-MgO were synthesized via wet impregnation using commercial γ-Al_2O_3 and MgO, respectively. The MgO was prepared through a batch co-precipitation method as previously reported.[72] Pd-HTs (**A** - **G, Table 3)** were synthesized using a mesoscale continuous flow precipitation method, adapted from our previously reported

protocol for flow synthesis of HTs.[73] The Pd-free Mg-Al HT was also synthesized in the same manner as a control HT. The compositions of **A** - **G** were highly reproducible, with standard deviations <5% of reported molar metal content. Elemental analysis by ICP-OES showed that the actual metal compositions were within 5% of the nominal values (**ESI Table S1**). A decrease in the M^{2+}/M^{3+} ratio (ideal ratio = 3.0) is observed for a few of the Pd-HTs doped with transition metals. This decrease is a result of the dopants ionic radius, whereas +2 metals with ionic radii larger than that of Mg^{2+} induce defects sites.

PXRD confirmed the presence of a single hydrotalcite phase for all Pd-xHTs. This phase is characterized by (003), (006), (009), (015), (018), (110), and (113) reflections (identified as reflections from left to right in Supporting Info Figure S4). No detectable crystalline Pd or PdO phases were observed for any of the Pd-HT's. The lack of any crystalline Pd phases, even at mol% Pd content, suggests that the palladium is highly dispersed either as a low-nuclearity species, or particles with sub 2-nm dimensions. The (003), (006), (009) reflections of the HT are sensitive to the interlayer spacing (crystallographic parameter *c*), while the (110) and (113) reflections are related to the average metal-metal distance within the metal cation layers (crystallographic parameter *a*). The consistent values of *a* and *c* parameters for all HTs suggest that a common, crystalline HT structure was obtained in each case and Pd functionalization had little to no impact on the structure of the support. The Scherrer equation was used to determine crystallite sizes, which were also consistent across all HTs synthesized (10.8 ± 0.8 nm). FT-IR spectra were indicative of a hydrotalcite phase, with characteristic bands for carbonate anions (1350 − 1370 cm^{-1}) and interlayer water (~1600-1700 cm^{-1}) (**ESI Figure S3).**

BET surface areas and BJH pore sizes for **A** − **G** were determined by nitrogen porosimetry (**ESI Table S2**). Although an increase in surface area and pore volume generally results in an increase of catalytic activity, no clear correlation was observed between surface area/pore volume and catalytic activity. We previously reported that pore volume decreases with increasing Pd loading[52] which is consistent with blockage of micropore entrances to interlayer spaces at higher loadings. However, the effects of transition metal doping on surface area and pore size aren't fully understood and further investigation is ongoing.

TGA analysis of all Pd-xHT's show materials that exhibit thermal decomposition profiles characteristic of HTs,[74] with three endothermic transitions at ~100 ^{o}C (physisorbed water), 200 - 250 ^{o}C, (loss of interlayer water), and 375 - 400 ^{o}C (dehydroxylation and the loss of interlayer carbonate anions)[64] (**ESI Figure S6**). These transitions occur within a relatively narrow range for **A** – **G**, but a decrease in temperature of the transitions is apparent for the doped Pd-xHT's relative to Pd-free HTs. This is especially true for transition III (dihydroxylation/decarbonation), as Pd likely destabilizes cation substitution and causes corresponding structural disorder.[75] We were not able to corroborate such intralayer substitution with PXRD data unfortunately, likely due to the low Pd loading.

TEM images of **B** – **G**, Pd-Al_2O_3, and Pd-MgO show that the Pd is uniformly distributed with 1.0 - 3.0 nm particles (**Figure 2**). This small particle size is consistent with the lack Pd features observed in PXRD. We previously reported an in-depth characterization on Pd-HT with nominal Pd loadings of 0.1, 0.5, 1.0 and 5.0 %.[53] Generally, a Pd loading greater than 1.0 % results two types of NP's: Pd (111) and PdO (110) phases, which was consistent with our findings for **B** – **G.** The largest particles were observed on Pd-NiHT, with mean size of 5.3 nm. In contrast to the Pd-HT, Pd-Al_2O_3 has only metallic Pd (111) species. No lattice fringes could be observed for Pd-MgO, and hence the nature of the corresponding Pd phase could not be directly assigned; however, PXRD identified reflections consistent with PdO (101), (112) and (220) planes (**ESI Figure S5b**). We thus propose that 5% Pd-xHT's (**B** - **G**) consists of atomically dispersed Pd^{4+} species incorporated into the HT cationic layers, low nuclearity Pd^{2+} species incorporated into the cationic layer or dispersed over the surface of HT layers, and Pd^{0} agglomerates on the surface. Determination of Pd dispersion through common experimental means such as CO chemisorption could not be employed as this approach requires that CO titrates only Pd metal and not the support. However, weakly acidic CO molecules can bind to hydrotalcites as they are solid bases, thus hindering accurate dispersion measurements. Consequently, catalytic activity is quantitated based on the total Pd content, consistent with previous reports[76-78] and hence reported TONs could underestimate the true catalyst performance.

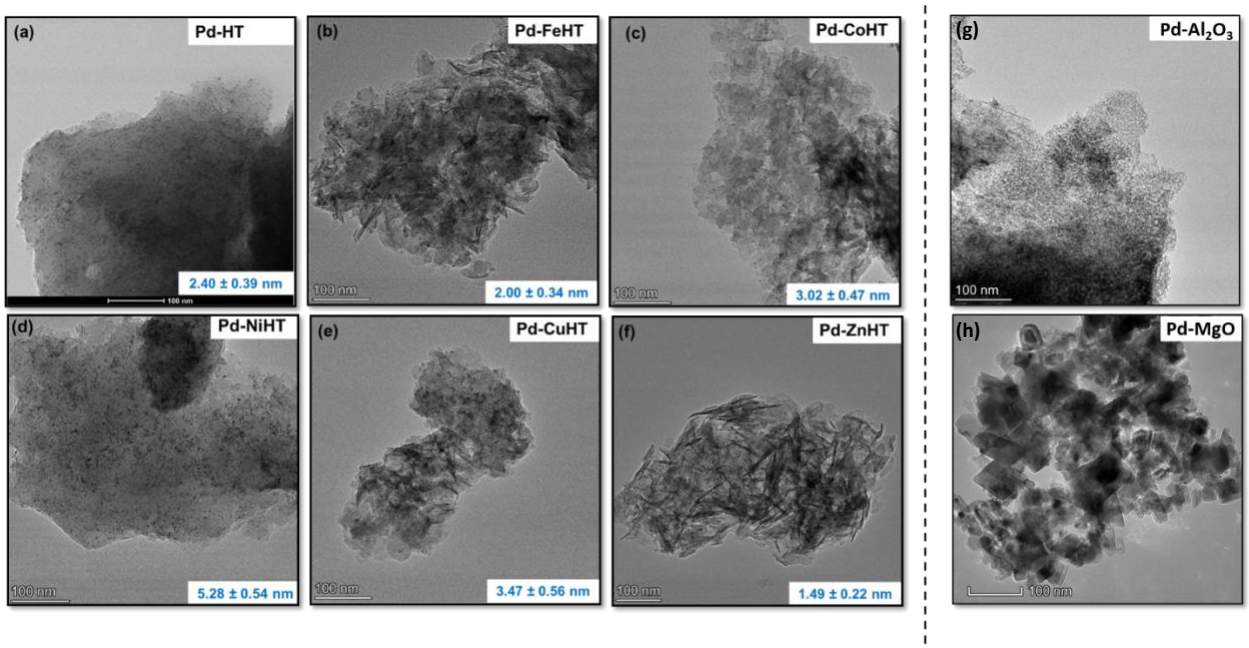

Figure 2. TEM images of (a) Pd-HT, (b) Pd-FeHT, (c) Pd-CoHT, (d) Pd-NiHT, (e) Pd-CuHT, (f) Pd-ZnHT, (g) Pd-Al_2O_3, and (h) Pd-MgO

Model Compound Studies

To test the activity of heterogeneous catalysts for defunctionalization of lignin motifs, model substrates of α-O-4 (L-**1**), β-O-4 (L-**2** to L-**4**), and 4-O-5 (L-**5**) linkages (**Figure 1**) were synthesized, along with several analogs lacking methoxy functionalization.

α-O-4

Benzyl phenylether (**L1**) was used as the simplest model substrate for probing the relative activity of the catalysts for transfer hydrogenolysis of α-O-4 linkages. Isopropanol, ethanol and glycerol were considered as hydrogen donor solvents. Initial results with 5%Pd-HT afforded ~80% yield of clean hydrogenolysis products with isopropanol in 2 hours at 150 °C using microwave heating (Table 2, entry 1), compared to 60% with ethanol (Table 2, entry 2); this is consistent with the expected more favorable kinetics and thermodynamics associated with dehydrogenation of a secondary alcohol (isopropanol) vs that of a primary (ethanol). Glycerol on its own was too viscous to be an effective solvent, and so was tested in 1:1 dilution with water. The latter afforded low yields (Table 2, entry 5). To probe whether dilution with water contributes to the low yields vs the viscosity of glycerol, we carried out an experiment with 1:1 isopropanol/water, which

Table 2. Effect of solvent for the Transfer Hydrogenolysis of Benzyl Phenylether (L-1) (α-O-4 linkage)

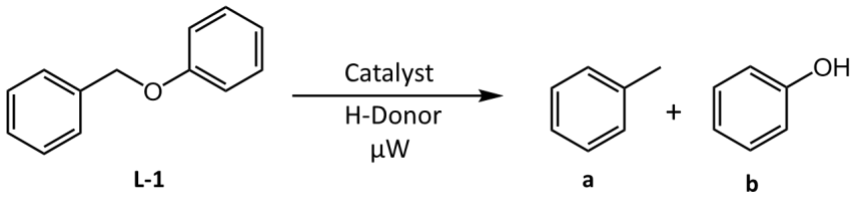

L-1 a b

Entry	Solvent	Conversion (%)	Yield (%)	
			a	b
1	Isopropanol	80	80	78
2	Ethanol	62	62	61
3	Isopropanol:Water (1:1)	53	53	50
4	Isopropanol:Glycerol (1:1)	50	50	50
5	Glycerol:Water (1:1)	12	10	10

Reaction conditions: Substrate: benzyl phenyl ether (L-1) (0.1 mmol), solvent (3.0 mL), catalyst: Pd-HT (5 mol%), μW heating at 150 ˚C, 2h.

afforded a ~30% yield reduction compared to a the reaction with neat isopropanol (Table 2, entry 3). In comparison, a reaction with 1:1 isopropanol and glycerol afforded comparable yields (Table 2, entry 4). The latter is consistent with the conclusion that glycerol is not an effective hydrogen donor for this reaction not due to its viscosity but due to the unfavorable dehydrogenation of glycerol. We note that this may change in the presence of base, which is critical for driving the conversion of the initial dehydrogenation product, dihydroxyacetone, to the more thermodynamically stable product lactate.[79-81]

The byproducts of the hydrogen donor solvents were briefly investigated. While isopropanol affords acetone, ethanol affords ethyl acetate. The inert nature of the ethanol byproduct may be an advantage in lignin-related reactions, as reactive aldehydes and ketones may undergo aldol reactions with carbonyls formed from β-O-4 linkers, resulting in a decrease of the selectivity of the overall reaction.

Table 3. Catalytic Activity for the Cleavage of Benzyl Phenyl Ether (L-1) via Transfer Hydrogenolysis

Entry	Catalyst	Conversion (%)	Yield (%)	
			a	b
1	HT **(A)**	0	0	0
2	5% Pd-HT **(B)**	62	62	61
3	5% Pd-FeHT **(C)**	68	68	67
4	5% Pd-NiHT **(D)**	71	70	68
5	5% Pd-CoHT **(E)**	89	89	88
6	5% Pd-CuHT **(F)**[1]	100	99	98
7	5% Pd-ZnHT **(G)**[1]	100	99	97
8	$Pd(OAc)_2$	0	0	0
9	3% Pd-Al_2O_3	0	0	0
10	3% Pd/C	30	29	27
11	3% Pd/MgO	34	33	32

Reaction conditions: Substrate: benzyl phenyl ether (**L-1**)(0.1 mmol), ethanol (3.0 mL), catalyst (5 mol %), μW 150 ˚C, 2h. [1] Reaction time decreased to 15 min.

We thus proceeded with a catalyst screen of transfer hydrogenolysis of benzyl phenyl ether (L1) using ethanol as the hydrogen-donor solvent, microwave heating at 150 ^{o}C for 2 and 5 mol % Pd loading relative to the model compound. The conversion and product yields of doped Pd-HTs (**A-G)** and several commercial heterogeneous Pd catalysts is reported in Table 3, with toluene and phenol as the only products observed. The Pd-free hydrotalcite (HT, **A**) afforded no conversion under these conditions, as did commercial palladium acetate and 3% Pd/Al_2O_3 (entries 1, 8 and 9). Low conversions were obtained with commercial 3% Pd/MgO and 3% Pd/C of ~30% (entries 10-11). Howveer, all Pd-xHT's afforded high conversion (62-100%), with Pd-CuHT (**F**) and Pd-ZnHT (**G**) affording quantitative conversion and yields of phenol and toluene. To further differentiate the performance of **F** and **G**, we decreased reaction time to 15 minutes, which still afforded quantitative conversion with the two catalysts. The relative activity of the doped Pd-HTs for the

transfer hydrogenolysis of benzyl phenyl ether hydrogenolysis using ethanol can be summarized as follows:

Pd-CuHT (**F**) ~ Pd-ZnHT (**G**) > Pd-CoHT **(E)**> Pd-NiHT **(D) >** Pd-FeHT **(C) > P**d-HT **(B)**

We postulated that the activity of the doped Pd-HTs is due to the ability to facilitate the first step – alcohol dehydrogenation. In the absence of substrate each of the catalysts in Table 3 was tested with ethanol and products tested by GC-MS. Small amounts of ethyl acetate and acetaldehyde were detected in the reactions with Pd-HTs, and no products were observed in the reactions with the commercial Pd catalysts. While not quantitative, this result is consistent with our hypothesis.

β-O-4 Model Compounds: *2-Phenoxyacetophenone*

The most abundant linkage in the lignin structure, β-O-4, can undergo additional transformations prior to ether cleavage, including dehydrogenation, dehydroxylation, transfer hydrogenolysis, and decarbonylation of the α and γ hydroxy post-dehydrogenation. Generally, these transformations are thermodynamically favorable and are known to weaken the ether bond.[41] In an effort to untangle the multi-step process, we first simplified β-O-4 model to 2-phenoxyacetophenone (**L2**), which allowed us to focus on the cleavage alone (**Scheme 1**). **L2** was subjected to catalysts (**A-G**) under the same conditions as the catalyst screen for **L1** (Supporting Info Table S3). As anticipated, the trends observed were consistent with those obtained with L1, with Pd-CuHT (**G**) affording highest activity (98% conversion and >90% selectivity).

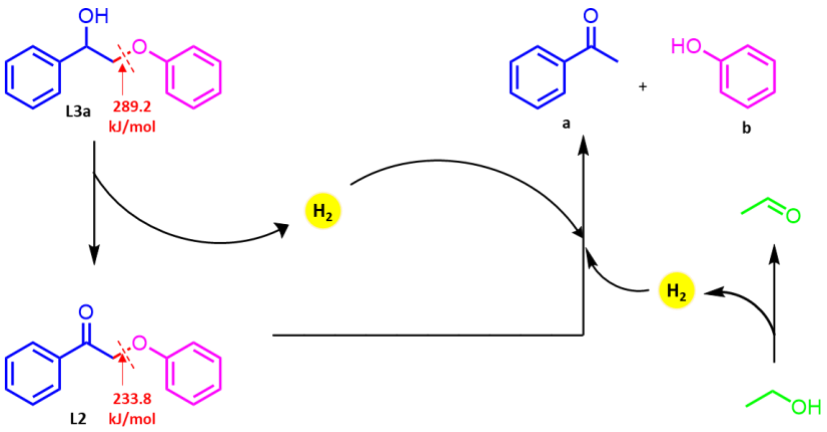

Scheme 1. Reaction Pathway for the conversion of 2-phenoxy-1-phenethanol (**L3a**) to acetophenone (a) and phenol (b) with doped Pd-HTs.

In comparison to the full selectivity observed for the benzyl phenyl ether, the slight drop in selectivity observed for 2-phenoxy-1-phenethanol is due to the two additional reactions taking place: transfer hydrogenation of the ketone, expected to occur after ether cleavage occurs, and aldol condensation of acetophenone, and possibly acetaldehyde (direct product from dehydrogenation of ethanol). At reaction temperatures above 150 ^{o}C both additional reactions become more prevalent (Figure 4c), decreasing selectivity. Further investigation into the effects of time and temperature was completed for the more complex model compounds introduced below.

β-O-4 Model Compounds: *2-Phenoxy-1-phenethanol (L3a)*

Motifs of the β-O-4 type found in lignin are natively found in the reduced state as compared to 2-phenoxyacetophenone (**L2**), which is oxidized form of 2-phenoy-1-phenethanol (**L3a)**. **L3a** was used to probe the catalysts multifunctional reactivity under the same conditions as for **L1** and **L2.** The benzylic hydroxyl group in **L3a** introduces more complexity from both a thermodynamic and kinetic standpoint. Thermodynamically, computational studies suggest that the ether bond dissociation energy decreases by ~55 kJ/mol after oxidation to the ketone (Reduced BDE: 289.2 kJ/mol vs oxidized BDE: 233.8 kJ/mol)[41] (**Scheme 1**). Thus, the catalysts must be active for both acceptorless dehydrogenation and ether transfer hydrogenolysis. The conversion and yields for the multistep transformation of **L3a** using catalysts **A, B, C, F** and **G** are presented in Table 4. Shown previously to be inactive for transfer hydrogenolysis of the ether bond (Table 3), the parent HT (**A**) is also inactive for dehydrogenation of the benzylic alcohol. Both 5% Pd-FeHT (**C**) and 5% Pd-CuHT (**F**) afford conversion >97%, however 5% Pd-CuHT (**F**) affords higher selectivity, with yields of 91% and 97% for **a** and **b**, respectively. For the cleavage step alone, 5% PdFeHT, 5% Pd-CuHT, and 5% Pd-ZnHT have continuously shown comparable results. However, the necessity for a dehydrogenation step has differentiated 5% Pd-CuHT as a more effective multifunctional catalyst for these specific transformations.

Experimental observations confirm that cleavage only occurs after dehydrogenation of the benzylic hydroxyl group. Based on this assumption, **a** and **b** would be the expected products after cleavage, which is what is observed as the major products reactions with catalysts **B, C, F, and G**.

However, cleavage could occur prior to oxidation giving compound **b** and **c**, whereas **c** is then oxidized post-cleavage to give **a**. When using 5% Pd-CuHT (**F**) the yield of **a** is 91% and compound **c** is 2%. Given these values, if oxidation was occurring post cleavage, **c** is readily oxidized to **a.** Therefore, a pure sample of **c** was subjected to the same conditions in the presence of 5% Pd-CuHT (**F**) in an effort to probe whether dehydrogenation is feasible. Negligible amounts of **a** were observed, leading us to conclude that cleavage occurs only after oxidation of the benzylic hydroxyl group (**Scheme 1**). Furthermore, the presence of **c** is attributed to hydrogenation of the carbonyl. This dehydroegantion and re-hydrogenation may also be occurring reversibly prior to cleavage, but **L2** is rarely observed in any appreciable yields, suggesting that once **L3a** is oxidized to **L2**, cleavage is rapid. Additionally, the introduction of a hydroxyl motif allows hydrogen to be sourced both from the solvent (ethanol) and intramolecularly via dehydrogenation. The degree to which intramolecular hydrogen plays a role is explored in more detail during reactions with **L5.**

Table 4. **Catalyst Screen for the Two Step Conversion of 2-Phenoxy-1-Phenethanol (L3a)**

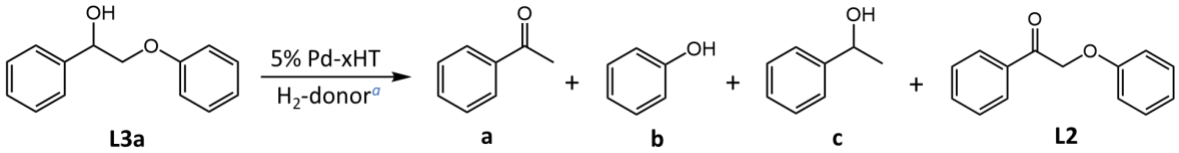

Entry	Catalyst	Conversion (%)	Yield (%)			
			a	b	c	d
1	HT **(A)**	1	0	0	0	1
2	5% Pd-HT **(B)**	39	29	34	7	2
3	5% Pd-FeHT **(C)**	97	67	79	15	4
4	5% Pd-CuHT **(F)**	100	91	97	2	0
5	5% Pd-ZnHT **(G)**	27	13	16	9	6

Reaction Conditions: Substrate: 2-phenoxy-1-phenethanol (0.1 mmol), ethanol (3.0 mL), catalyst (5 mol %), µW 150 ˚C, 2h. [a]The hydrogen can be sourced through dehydrogenation of ethanol or intramolecularly through dehydrogenation of the substrate.

Thus far, 5% Pd-CuHT (**F**) has been shown to have highest activity for both of the major steps outlined, and was thus taken forward for further optimization and exploration of more complex model substrates that are more representative of native lignin. 1-(3,4-Dimethoxyphenyl)-2-(2-methoxyphenoxy)-1,3-propanediol (**L3b**) was used as a model compound to explore the effects of methoxy functionalities which are common to lignin. Catalyst loading (1 mol %, 2.5 mol % and 5 mol %) was explored first (**Figure 4b**). Under these conditions, a 2.5 mol % loading of 5% Pd-CuHT exhibits the highest conversion (65%) and selectivity to **d** and **e** of 88% and 91%, respectively. Any loss in selectivity was generally a result of hydrogenation of **d**, which was observed for the reactions with **L3a** as well**.** The presence of methoxy groups does not reduce selectivity, but does decrease conversion, even with a 5 mol % loading. Although the three loadings afforded similar conversions, we chose to move forward with a 2.5 mol % loading based on the high degree of selectivity. The effect of temperature was studied next (**Figure 4c**). Conversion steadily increases from 130 ^{o}C (62%) to 160 ^{o}C (82%), while the same trend observed for selectivity from 130 ^{o}C to 150 ^{o}C, shows a decrease at 160 ^{o}C. Selectivity decreases due to dehydrogenation of **d** to 3,4-dimethoxylated analog of **c**, in addition to aldol condensation products. Even though 150 ^{o}C does not afford highest conversion (72%), excellent selectivity (**d**: 96%, **e**: 93%) is observed at this temperature. As expected, opposite trends between temperature, conversion and selectivity are observed, necessitating optimization to achieve both. Gratifyingly, by increasing reaction time to 6 hours (150 ^{o}C, 2.5 mol % catalyst loading, **Figure 4d**) we were able to obtain 95% selectivity and quantitative conversion (yields of 90% for **d** and 93% for **e**). Interestingly, computational studies have shown that the addition of methoxy groups are thermodynamically favorable, however experimental evidence shows they hinder kinetics of ether bond cleavage.

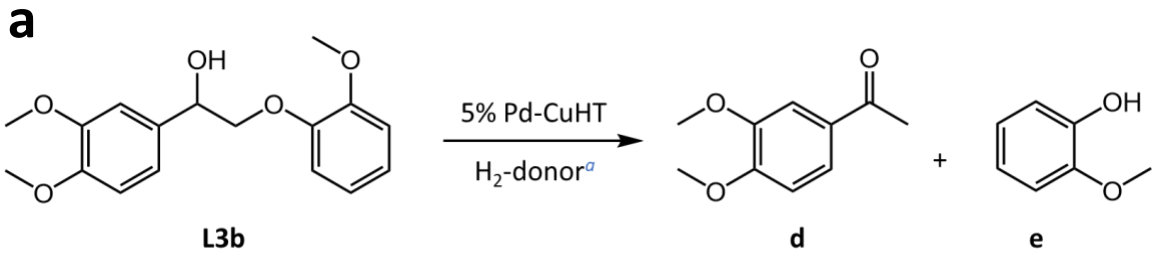

[a]The hydrogen can be sourced through dehydrogenation of ethanol or intramolecularly through dehydrogenation of the substrate.

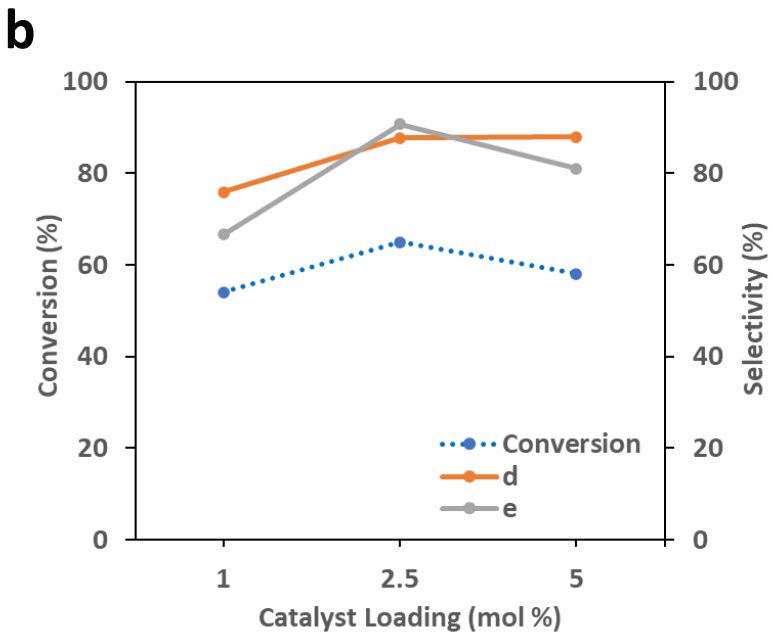

Reaction Conditions: Substrate: L3b (0.1 mmol), ethanol (3.0 mL), 5% Pd-CuHT, µW 130 ˚C, 2 h.

c

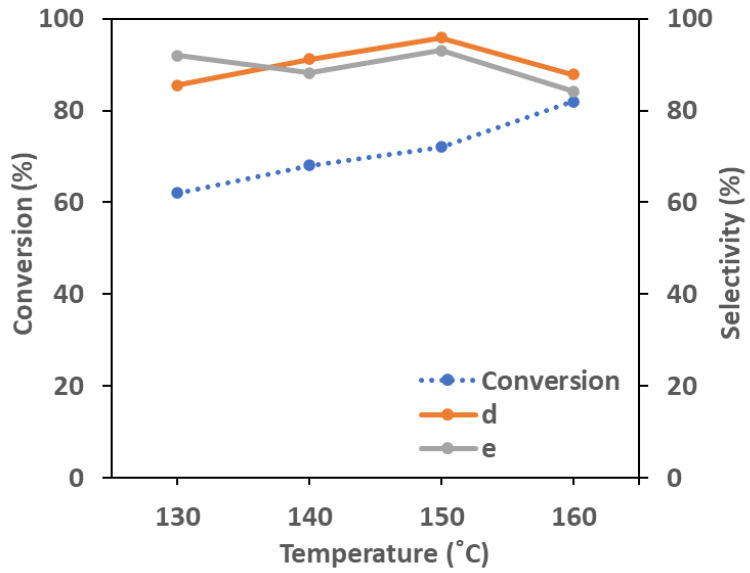

Reaction Conditions: Substrate: L3b (0.1 mmol), ethanol (3.0 mL), 2.5% Pd-CuHT, µW, 2 h.

d

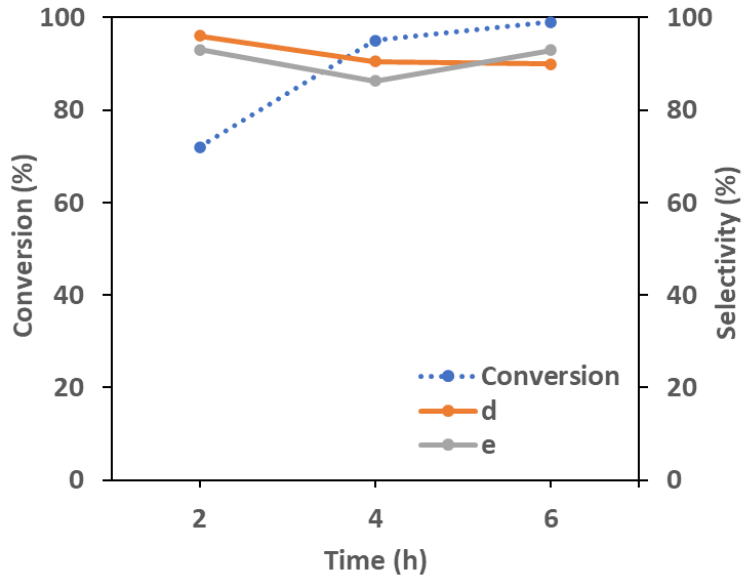

Reaction Conditions: Substrate: L3b (0.1 mmol), ethanol (3.0 mL), 2.5% Pd-CuHT, µW 150 ˚C.

Figure 4. General reaction scheme (a) with optimization of reaction parameters for the conversion of L3b: (b) catalyst loading, (c) temperature, and (d) and time.

Effect of γ-Hydroxy Group – C3 Type Model Compound (L5)

Table 5. Transfer Hydrogenolysis of L4 Model Compound with Additional *γ*-Hydroxy Group

Entry	Solvent	Conversion (%)	Yield (%)		
			h	d	e
1	*p*-Xylene	88	75	5	4
2	Dioxane	13	11	2	1
3	EtOH	98	7	90	93

Reaction Conditions: Substrate: L5 (0.1 mmol), solvent (3.0 mL), 2.5% Pd-CuHT, µW 150 ˚C.

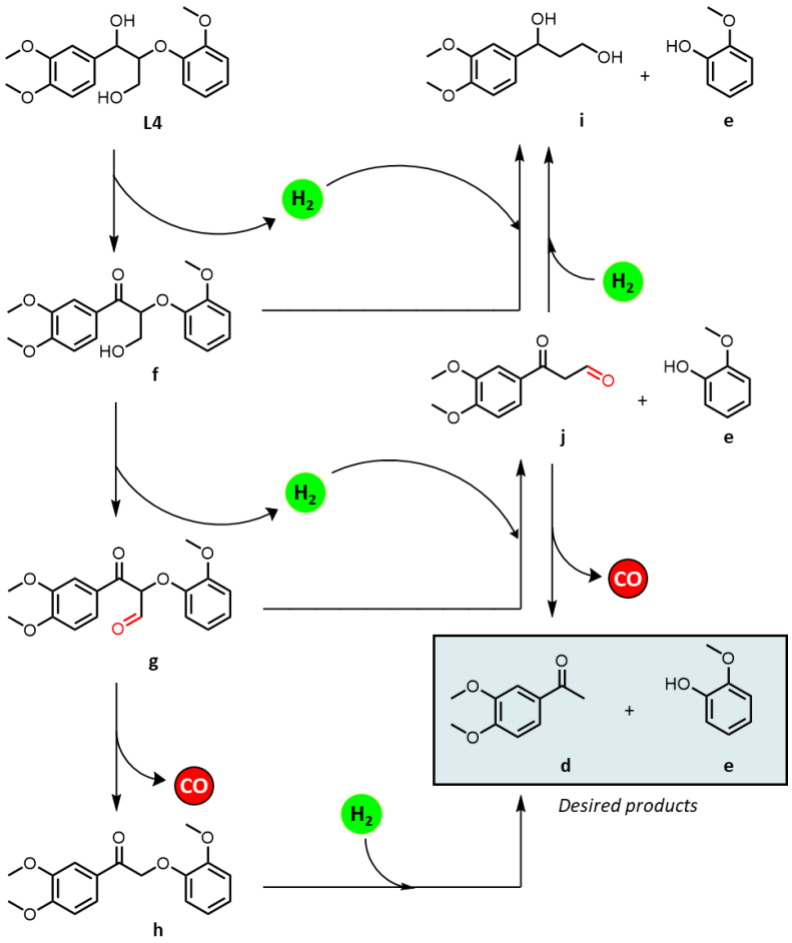

Scheme 2. Proposed reaction pathway for the multi-step transformation of **L5**.

L4 was employed as a C3 model type compound to investigate the impact of additional functional groups (Table 5). The major point of interest with the C3 type model compounds is the effect of the γ-hydroxymethyl group which adds an additional layer of complexity to this reaction and better represents lignin in its native form. Under the optimized conditions of 150 ˚C with a 2.5 mol% loading of 5% Pd-CuHT a conversion of 98% was achieved, with a selectivity to **d** and **e** of 90% and 93%, respectively. Scheme 2 shows the proposed reaction pathway to the desired products. It is hypothesized that the γ-hydroxy group is oxidized to an aldehyde which is successively lost via decarbonylation. Our group has previously reported that 5% Pd-HT shows excellent decarbonylation activity.[53] Decarbonylation can occur before or after cleavage, although, oxidation of both the benzylic and gamma hydroxy groups is thermodynamically favorable for cleavage to occur.[41] Oxidation of at least one of the hydroxy groups has shown to be necessary for cleavage to occur, but the benzylic hydroxy group exists as a secondary alcohol which is thermodynamically favorable for dehydrogenation as compared to the primary gamma hydroxy group. The product distributions suggest that indeed, both hydroxy groups are oxidized followed by decarbonylation of the aldehyde before cleavage as **h** is isolated in much higher yields than **I** or **j.** After decarbonylation, the structure is that of L2 and therefore see the same breakdown pathway as seen previously.

This reaction was also carried out using dioxane and *p*-xylene which are both non hydrogen donating solvents. The purpose was to explore to what extent intramolecular hydrogen was being used for hydrogenolysis of the ether bond. *p*-Xylene shows comparable conversion to ethanol (88% vs. 98%), however yields of both **d** and **e** are 5% or less. Dioxane gives a much lower conversion (13%), but very similar product distribution to *p*-xylene. In both cases the major product was **L2**, which indicates that the existence of a hydrogen donating solvent is the major source of hydrogen needed for hydrogenolysis. Since **d** and **e** are observed for both *p*-xylene and dioxane, intramolecularly sourced transfer hydrogenolysis must be occurring. However, the rate at which it is occurring is inhibitory to achieve reasonable reaction times. Overall, the solvent plays an important role, but a hydrogen donating solvent such as ethanol increases the kinetics drastically.

Cleavage of 4-O-5 Compounds

Diphenyl ether (L5) was used as a model compound to represent the 4-O-5 linkage found in lignin (Table 6). Naturally, due to the connectivity of this structure, it was anticipated that cleavage of either Ph-O bond would be more difficult than α-O-4 or β-O-4 ether bonds. Results confirmed this, obtaining a highest conversion of 23% with 5% Pd-HT (**Table 6, Entry 1**) even at a slightly higher temperature and longer reaction time. However, even 23% conversion is promising as this type of linkage has been notoriously difficult to deal with. Efforts continue to further increase the hydrogenolysis activity of Pd-xHt's for this type of linkage.

Table 6. Transfer Hydrogenolysis of Diphenyl Ether (L5)

Entry	Catalyst	Solvent	Conversion (%)
1	Pd-HT	EtOH	12
2	Pd-HT	iPrOH	23
3	Pd-CuHT	EtOH	15
4	Pd-CuHT	iPrOH	8

Reaction conditions: Substrate (L5)(0.1 mmol), solvent (3.0 mL), catalyst (5.0 mol %), μW 150 ˚C, 4h.

Applications for Whole Biomass ("Lignin First" Approach to Depolymerization)

Recently, an old approach has come back into the spotlight in an effort to increase the value of lignin phenolic units. The general route to attacking lignin is taking advantage of the high degree of ether linkages. Cleaving these bonds in native lignin is a feasible task, however, during common extraction methods (ie. Kraft, organosolv, etc.) the lignin takes on an even more calcitrant structure.[82] Reactive intermediates are responsible for forming new C—C bonds that become overly difficult to break[83], especially in a selective manner. Reductive Catalytic Fractionation (RCF) is the process of using a reductive heterogenous metal catalyst during the extraction process.[84] The metal catalyst stabilizes the reactive intermediates, inhibiting further condensation reactions while additional depolymerization is allowed to take place. RCF is a two-step process: (i) lignin extraction from whole biomass with a polar-protic solvent (ethanol is this case), and then (ii) selectively cleaving C-O ether bonds using a hydrogen donor (from ethanol) and a heterogeneous catalyst (5% Pd-HT).[85] Instead of extracting lignin and subsequently attempting to selectively

depolymerize what is now a technical lignin, the extraction and depolymerization happen simultaneously. This approach (outlined in figure 5) is now colloquially called the "lignin first" approach and several reviews have covered this strategy in depth.[2, 83-89]

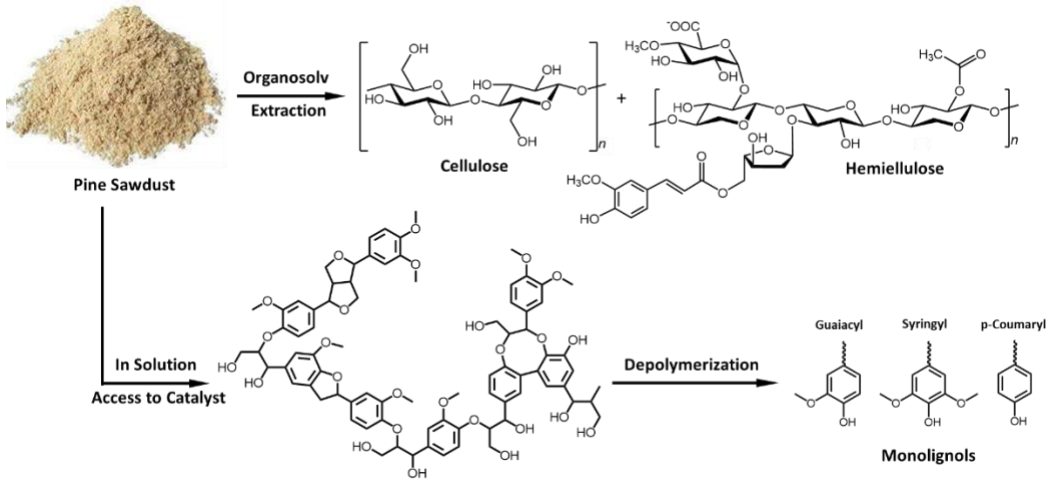

Figure 5. Proposed reaction scheme for the extraction of lignin from whole biomass followed by subsequent depolymerization. This process occurs simultaneously in a single

Table 7. Reductive Catalytic Fractioning of Whole Pine Biomass using Hydrotalcite Supported Palladium

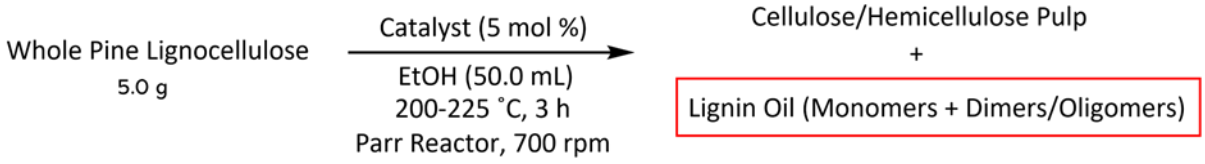

Entry	Catalyst	Temperature (˚C)	Phenolic Product Yield (%)[a]			Delignification [b] (%)
			HA[c]	Other Monomers	Dimers	
1	5% Pd-HT	200	23	11	3	82
2	5% Pd-HT	225	33	6	4	82
4	N/A	200	0.5	<1	<1	72

Reaction Conditions: Parr autoclave, pine sawdust (5.0 g), ethanol (50.0 mL), 5% Pd-HT (0.6 g), 3 h. [a] The degree of depolymerization to monomer units through this process is based on the amount of ether type linkages (b-O-4, a-O-4, etc.). Pine is reported to have a maximum monomer yield of ~35-40-% (See Supporting Info for detailed explanation of theoretical monomer yield and monomer yield determination).[18, 90] Monomer yield is a percentage of the theoretical lignin present as a whole, not just a percentage of the lignin extracted. [b] Pine wood was determined to possess 32% lignin by weight. [c] Hydro coniferyl Alcohol

Whole pine RCF reactions were carried out in a Parr autoclave reactor at temperatures from 200-225 ˚C using 5% Pd-HT. Base Pd-HT instead of Pd-CuHT was used based on literature precedence which states Pd itself is a great reductant for reactive intermediate stabilization. Therefore, before moving onto doped HT's, 5% Pd-HT was used as an initial test. A control reaction with no catalyst (Table 7, Entry 4) was carried out, which is essentially an organosolv extraction. Not surprisingly, over 70% of the lignin was extracted, however, monomer and dimer yields were less than 1%. As mentioned above, without a catalyst any ether bonds that are broken form reactive intermediates that subsequently form new C—C bonds, thus making a technical lignin. Access to quantitative details for polymers was limited, therefore values such as average molecular mass and polydispersity could not be obtained. Nonetheless, the poor monomer, dimer, and even oligomer yield suggests that the lignin still largely has a high molecular mass meaning depolymerization is profoundly restricted. The reaction was then carried out with the addition of 5% Pd-HT at two different temperatures, 200 ˚C (Table 7, Entry 1) and 225 ˚C (Table 7, entry 2). In both cases, delignification itself was increased to 82% and at 225 ˚C a 39% monomer yield was obtained which is close to the theoretical maximum. The major product observed was hydroconiferyl alcohol (HA) which is a guaiacyl derived monolignol of which lignin in pine wood primarily consists of.[90] Surprisingly, the selectivity (85%, in reference to all monomers observed) towards this compound was higher than anticipated. Two other compounds regularly observed were ethyl guaiacol and propyl guaiacol, both guaicyl monolignols. These results suggest that the HA comes from cleavage of β-O-4 linkages, while ethyl and propyl guaiacol are from α-O-4 linkages. Due to the complex nature of lignin, the true mechanism by which the catalyst is behaving has not yet been established and further investigation is needed. Regardless, palladium hydrotalcite has shown to be effective for reductive catalytic fractionation of lignin through a "lignin first approach". For pine biomass, the obtained monomer and delignification yields are analogous to literature precedence with the advantage of sourcing hydrogen directly from the solvent.

Conclusions

Lignin model substrates of α-O-4 (L-**1**), β-O-4 (L-**2** to L-**4**), and 4-O-5 (L-**5**) linkages (**Figure 1**) were used to probe the catalytic activity of Pd-HTs. Benzyl phenylether was used as substrate for an extensive screen of Pd-HT catalysts to determine the efficiency for transfer hydrogenolysis using ethanol as hydrogen donor. The initial catalyst screen identified Pd-CuHT and Pd-ZnHT as the most active catalyst for benzyl phenylether, achieving full conversion using ethanol at 2 hours at 150°C with Pd-CuHT and Pd-ZnHT. ***This is the first system effective with ethanol as H-donor. In addition, no base is required which is critical for making the system potentially economically viable.*** Similarly, a screen for the reactions that cleave the β-O-4 linker identified the same catalyst, Pd-CuHT, as the most active and selective catalyst for both C2 and C3 type β-O-4 compounds. Extensive further optimization of reaction conditions has been carried out, as well as structure-activity studies to elucidate how catalytic activity for the multi-step process can be rationally optimized. Finally, for the 4-O-5 linkage, the biphenyl ethers, current screens find the catalyst only affords 25% conversion. This is not surprising given the challenging nature of transfer hydrogenolysis of biphenyl ethers. Further catalyst optimization is ongoing for this linkage.

References

1. P. Anastas, M. Nolasco, F. Kerton, M. Kirchhoff, P. Licence, T. Pradeep, B. Subramaniam and A. Moores, *Acs Sustain Chem Eng*, 2021, **9**, 8015-8017.
2. R. Rinaldi, R. Jastrzebski, M. T. Clough, J. Ralph, M. Kennema, P. C. A. Bruijnincx and B. M. Weckhuysen, *Angewandte Chemie Int Ed*, 2016, **55**, 8164-8215.
3. Y. Song, J. K. Mobley, A. H. Motagamwala, M. Isaacs, J. A. Dumesic, J. Ralph, A. F. Lee, K. Wilson and M. Crocker, *Chem Sci*, 2018, **9**, 8127-8133.
4. Z. Sun, B. Fridrich, A. d. Santi, S. Elangovan and K. Barta, *Chem Rev*, 2018, **118**, 614-678.
5. R. Parthasarathi, R. A. Romero, A. Redondo and S. Gnanakaran, *J Phys Chem Lett*, 2011, **2**, 2660-2666.
6. K. Barta, G. R. Warner, E. S. Beach and P. T. Anastas, *Green Chemistry*, 2014, **16**, 191-196.
7. J. Chen, F. Lu, X. Si, X. Nie, J. Chen, R. Lu and J. Xu, *ChemSusChem*, 2016, **9**, 3353-3360.
8. P. Ferrini and R. Rinaldi, *Angewandte Chemie Int Ed*, 2014, **53**, 8634-8639.
9. Y. Hu, G. Jiang, G. Xu and X. Mu, *Molecular Catalysis*, 2018, **445**, 316-326.
10. X. Huang, T. I. Korányi, M. D. Boot and E. J. M. Hensen, *ChemSusChem*, 2014, **7**, 2276-2288.
11. H. Konnerth, J. Zhang, D. Ma, M. H. G. Prechtl and N. Yan, *Chemical Engineering Science*, 2015, **123**, 155-163.
12. Z. Luo, Z. Zheng, L. Li, Y.-T. Cui and C. Zhao, *ACS Catalysis*, 2017, **7**, 8304-8313.
13. B. Ma, H. Cui, D. Wang, P. Wu and C. Zhao, *Nanoscale*, 2017, **9**, 5986-5995.

14. R. Ma, W. Hao, X. Ma, Y. Tian and Y. Li, *Angewandte Chemie Int Ed*, 2014, **53**, 7310-7315.
15. V. Molinari, C. Giordano, M. Antonietti and D. Esposito, *Journal of the American Chemical Society*, 2014, **136**, 1758-1761.
16. Y. Shao, Q. Xia, L. Dong, X. Liu, X. Han, S. F. Parker, Y. Cheng, L. L. Daemen, A. J. Ramirez-Cuesta, S. Yang and Y. Wang, *Nature Communications 2017 8:1*, 2017, **8**, 1-9.
17. L. Shuai, M. T. Amiri, Y. M. Questell-Santiago, F. Héroguel, Y. Li, H. Kim, R. Meilan, C. Chapple, J. Ralph and J. S. Luterbacher, *Science*, 2016, **354**, 329-333.
18. S. Van den Bosch, W. Schutyser, R. Vanholme, T. Driessen, S. F. Koelewijn, T. Renders, B. De Meester, W. J. J. Huijgen, W. Dehaen, C. M. Courtin, B. Lagrain, W. Boerjan and B. F. Sels, *Energy & Environmental Science*, 2015, **8**, 1748-1763.
19. Q. Xia, Z. Chen, Y. Shao, X. Gong, H. Wang, X. Liu, S. F. Parker, X. Han, S. Yang and Y. Wang, *Nature Communications 2016 7:1*, 2016, **7**, 1-10.
20. M. Zaheer and R. Kempe, *ACS Catalysis*, 2015, **5**, 1675-1684.
21. J. Zhang, H. Asakura, J. Van Rijn, J. Yang, P. Duchesne, B. Zhang, X. Chen, P. Zhang, M. Saeys and N. Yan, *Green Chemistry*, 2014, **16**, 2432-2437.
22. J. Zhang, J. Teo, X. Chen, H. Asakura, T. Tanaka, K. Teramura and N. Yan, *ACS Catalysis*, 2014, **4**, 1574-1583.
23. W. Deng, H. Zhang, X. Wu, R. Li, Q. Zhang and Y. Wang, *Green Chemistry*, 2015, **17**, 5009-5018.
24. Y. Gao, J. Zhang, X. Chen, D. Ma and N. Yan, *ChemPlusChem*, 2014, **79**, 825-834.
25. C. S. Lancefield, O. S. Ojo, F. Tran and N. J. Westwood, *Angewandte Chemie Int Ed*, 2015, **54**, 258-262.
26. R. Lu, F. Lu, J. Chen, W. Yu, Q. Huang, J. Zhang and J. Xu, *Angewandte Chemie Int Ed*, 2016, **55**, 249-253.
27. R. Ma, M. Guo and X. Zhang, *ChemSusChem*, 2014, **7**, 412-415.
28. M. Wang, X. Zhang, H. Li, J. Lu, M. Liu and F. Wang, *ACS Catalysis*, 2018, **8**, 1614-1620.
29. P. J. Deuss, M. Scott, F. Tran, N. J. Westwood, J. G. de Vries and K. Barta, *Journal of the American Chemical Society*, 2015, **137**, 7456-7467.
30. J. Hu, D. Shen, S. Wu, H. Zhang and R. Xiao, *Energy & Fuels*, 2014, **28**, 4260-4266.
31. T. D. H. Nguyen, M. Maschietti, T. Belkheiri, L.-E. Åmand, H. Theliander, L. Vamling, L. Olausson and S.-I. Andersson, *The Journal of Supercritical Fluids*, 2014, **86**, 67-75.
32. J. A. Onwudili and P. T. Williams, *Green Chemistry*, 2014, **16**, 4740-4748.
33. Y. Pan, R. Qiu, J. Li, L. Bi, B. Shang and J. Tschiersch, *Qinghua Daxue Xuebao/Journal of Tsinghua University*, 2013, **53**, 1380-1384.
34. A. Toledano, L. Serrano and J. Labidi, *Fuel*, 2014, **116**, 617-624.
35. L. Yang, Y. Li and P. E. Savage, *Industrial & Engineering Chemistry Research*, 2014, **53**, 2633-2639.
36. S. Adhikari, V. Srinivasan and O. Fasina, *Energy & Fuels*, 2014, **28**, 4532-4538.
37. G. Jiang, Y. Hu, G. Xu, X. Mu and H. Liu, *Acs Sustain Chem Eng*, 2018, **6**, 5772-5783.
38. G. T. Neumann, B. R. Pimentel, D. J. Rensel and J. C. Hicks, *Catalysis Science & Technology*, 2014, **4**, 3953-3963.
39. M. P. Pandey and C. S. Kim, *Chemical Engineering & Technology*, 2011, **34**, 29-41.
40. H. Liu, H. Li, J. Lu, S. Zeng, M. Wang, N. Luo, S. Xu and F. Wang, *ACS Catalysis*, 2018, **8**, 4761-4771.
41. J. D. Nguyen, B. S. Matsuura and C. R. J. Stephenson, *Journal of the American Chemical Society*, 2014, **136**, 1218-1221.
42. D. Shao, J. Liang, X. Cui, H. Xu and W. Yan, *Chemical Engineering Journal*, 2014, **244**, 288-295.
43. M. J. Gilkey and B. Xu, *ACS Catalysis*, 2016, **6**, 1420-1436.
44. C. Capello, U. Fischer and K. Hungerbühler, *Green Chemistry*, 2007, **9**, 927-934.
45. K. Tekin, N. Hao, S. Karagoz and A. J. Ragauskas, *ChemSusChem*, 2018, **11**, 3559-3575.

46. L. Jiang, H. Guo, C. Li, P. Zhou and Z. Zhang, *Chem Sci*, 2019, **10**, 4458-4468.
47. X. Wang and R. Rinaldi, *Energy & Environmental Science*, 2012, **5**, 8244-8260.
48. E. Paone, C. Espro, R. Pietropaolo and F. Mauriello, *Catalysis Science & Technology*, 2016, **6**, 7937-7941.
49. M. V. Galkin, C. Dahlstrand and J. S. M. Samec, *ChemSusChem*, 2015, DOI: 10.1002/cssc.201500117.
50. M. Crespo-Quesada, A. Yarulin, M. S. Jin, Y. N. Xia and L. Kiwi-Minsker, *J. Am. Chem. Soc.*, 2011, **133**, 12787-12794.
51. D. Ainembabazi, C. Reid, A. Chen, N. An, J. Kostal and A. Voutchkova-Kostal, *J. Am. Chem. Soc.*, 2020, **142**, 696-699.
52. D. Ainembabazi, N. An, J. C. Manayil, K. Wilson, A. F. Lee and A. M. Voutchkova-Kostal, *ACS Catalysis*, 2019, **9**, 1055-1065.
53. N. An, D. Ainembabazi, C. Reid, K. Samudrala, K. Wilson, A. F. Lee and A. Voutchkova-Kostal, *ChemSusChem*, 2020, **13**, 312-320.
54. M. A. Stranick, M. Houalla and D. M. Hercules, *J. Catal.*, 1990, **125**, 214-226.
55. A. Davantès, C. Schlaup, X. Carrier, M. Rivallan and G. Lefèvre, *J. Phys. Chem. C*, 2017, **121**, 21461-21471.
56. O. Borg, P. Dietzel, A. Spjelkavik, E. Tveten, J. Walmsley, S. Diplas, S. Eri, A. Holmen and E. Rytter, *J. Catal.*, 2008, **259**, 161-164.
57. B. N. Shelimov, J. F. Lambert, M. Che and B. Didillon, *J. Mol. Catal. A: Chem.*, 2000, **158**, 91-99.
58. F. Saad, J. D. Comparot, R. Brahmi, M. Bensitel and L. Pirault-Roy, *Appl. Catal., A*, 2017, **544**, 1-9.
59. B.-Q. Xu, T. Yamaguchi and K. Tanabe, *Chem. Lett.*, 1988, **17**, 1663-1666.
60. H. P. Aytam, V. Akula, K. Janmanchi, S. R. R. Kamaraju, K. R. Panja, K. Gurram and J. W. Niemantsverdriet, *The Journal of Physical Chemistry B*, 2002, **106**, 1024-1031.
61. W. Gac, *Appl. Surf. Sci.*, 2011, **257**, 2875-2880.
62. C. Poupin, R. Maache, L. Pirault-Roy, R. Brahmi and C. T. Williams, *Appl. Catal., A*, 2014, **475**, 363-370.
63. E. Groppo, S. Bertarione, F. Rotunno, G. Agostini, D. Scarano, R. Pellegrini, G. Leofanti, A. Zecchina and C. Lamberti, *J. Phys. Chem. C*, 2007, **111**, 7021-7028.
64. F. Cavani, F. Trifiro and A. Vaccari, *Catal. Today*, 1991, **11**, 173-301.
65. Y. He, P. Yang, J. Fan, Y. Liu, Y. Du, J. Feng, F. Fan and D. Li, *RSC Advances*, 2015, **5**, 74907-74915.
66. M. G. Álvarez, R. J. Chimentão, F. Figueras and F. Medina, *Applied Clay Science*, 2012, **58**, 16-24.
67. O. D. Pavel, D. Tichit and I.-C. Marcu, *Appl. Cl. Sci.*, 2012, **61**, 52-58.
68. J. Bain, P. Cho and A. Voutchkova-Kostal, *Green Chemistry*, 2015, **17**, 2271-2280.
69. D. Ainembabazi, J. Horlyck, D. Dolan, M. Finn, A. F. Lee, K. Wilson and A. Voutchkova-Kostal, *ACS Sust. Chem. & Eng.*, 2021, **9**, 14657-14662.
70. G. J. S. Dawes, E. L. Scott, J. Le Nôtre, J. P. M. Sanders and J. H. Bitter, *Green Chem.*, 2015, **17**, 3231-3250.
71. J. A. Lopez-Ruiz and R. J. Davis, *Green Chem.*, 2014, **16**, 683-694.
72. S. R. Akuri, C. Dhoke, K. Rakesh, S. Hegde, S. A. Nair, R. Deshpande and P. Manikandan, *Catalysis Letters*, 2017, **147**, 1285-1293.
73. P. Yaseneva, N. An, M. Finn, N. Tidemann, N. Jose, A. Voutchkova-Kostal and A. Lapkin, *Chem. Eng. J.*, 2019, **360**, 190-199.
74. R. Jules C. A. A, J. A. Bokhoven, J. A. van Dillen, J. W. Geus and K. P. de Jong, *Chemistry A European Journal*, 2002, **8**, 5571-5579.
75. J. Pérez-Ramírez, G. Mul and J. A. Moulijn, *Vibrational Spectroscopy*, 2001, **27**, 75-88.
76. N. Agarwal, S. J. Freakley, R. U. McVicker, S. M. Althahban, N. Dimitratos, Q. He, D. J. Morgan, R. L. Jenkins, D. J. Willock, S. H. Taylor, C. J. Kiely and G. J. Hutchings, *Science*, 2017, **358**, 223-227.

77. A. Corma, P. Concepción, M. Boronat, M. J. Sabater, J. Navas, M. J. Yacaman, E. Larios, A. Posadas, M. A. López-Quintela, D. Buceta, E. Mendoza, G. Guilera and A. Mayoral, *Nature chemistry*, 2013, **5**, 775-781.
78. J. K. Edwards and G. J. Hutchings, *Angewandte Chemie Int Ed*, 2008, **47**, 9192-9198.
79. A. Azua, M. Finn, H. N. Yi, A. B. Dantas and A. Voutchkova-Kostal, *ACS Sust. Chem. & Eng.*, 2017, **5**, 3963-3972.
80. M. Finn, J. A. Ridenour, J. Heltzel, C. Cahill and A. Voutchkova-Kostal, *Organometallics*, 2018, **37**, 1400-1409.
81. J. M. Heltzel, M. Finn, D. Ainembabazi, K. Wang and A. M. Voutchkova-Kostal, *Chem. Commun.*, 2018, **54**, 6184-6187.
82. S. Van Den Bosch, T. Renders, S. Kennis, S. F. Koelewijn, G. Van Den Bossche, T. Vangeel, A. Deneyer, D. Depuydt, C. M. Courtin, J. M. Thevelein, W. Schutyser and B. F. Sels, *undefined*, 2017, **19**, 3313-3326.
83. M. V. Galkin and J. S. M. Samec, *ChemSusChem*, 2016, **9**, 1544-1558.
84. T. Renders, S. Van den Bosch, S. F. Koelewijn, W. Schutyser and B. F. Sels, *Energy & Environmental Science*, 2017, **10**, 1551-1557.
85. W. Schutyser, T. Renders, S. Van den Bosch, S. F. Koelewijn, G. T. Beckham and B. F. Sels, *Chemical Society Reviews*, 2018, **47**, 852-908.
86. J.-M. Ha, K.-R. Hwang, Y.-M. Kim, J. Jae, K. H. Kim, H. W. Lee, J.-Y. Kim and Y.-K. Park, *Renewable and Sustainable Energy Reviews*, 2019, **111**, 422-441.
87. E. Paone, T. Tabanelli and F. Mauriello, *Current Opinion in Green and Sustainable Chemistry*, 2020, **24**, 1-6.
88. Y. Song, in *Chemical Catalysts for Biomass Upgrading*, 2020, DOI: https://doi.org/10.1002/9783527814794.ch9, pp. 395-437.
89. Z. Sun, B. Fridrich, A. de Santi, S. Elangovan and K. Barta, *Chem Rev*, 2018, **118**, 614-678.
90. M. V. Galkin and J. S. M. Samec, *ChemSusChem*, 2014, **7**, 2154-2158.

Acid-Base Method

The acid-base properties of the catalysts were studied by pulse titration of CO_2 and temperature programmed decomposition of propylamine, measured on a Quantachrome ChemBET system coupled to an MKS Minilab QMS and Mettler-Toledo Star2 thermogravimetric analyzer coupled to a Pfeffier Omnistar QMS respectively. Samples (200 mg) were degassed at 150 °C for 3 h, prior to saturation with CO_2 by pulse titration at 40 °C. Temperature-programmed decomposition of propylamine decomposition to propene and NH_3 via the Hoffman elimination reaction was also employed to independently quantify the acid loading. *n*-Propylamine (≥99 %, Sigma Aldrich) was added to just wet samples (10 mg) which were then dried for 2 h, and physisorbed propylamine removed by degassing at 30 °C overnight in vacuo. Samples were then heated in the thermogravimetric analyzer under flowing N_2 (30 cm^3/min) from 40- 1000 °C at a ramp rate of 10 °C/min. MS signals at 17 and 41 amu were followed to quantify evolved ammonia and propene respectively.

Acid-Base Results

Acid−base properties were determined by CO_2 titration and *n*-propylamine temperature programmed desorption (following the production of reactively formed propene via the Hoffman elimination), respectively. The total base site loading decreased monotonically with increasing Pd doping, accompanied by a concomitant rise in acidity (Figure 3), suggesting that Pd caps surface hydroxyls and introduces Lewis acidity in the form of Pdδ+ species. This includes the presence of Lewis acidic and basic sites inherent to HT's, whereby the ratio of acidic and basic sites in addition to their relative strength plays a major role in overall catalytic activity. This property can be tuned by the introduction of transition metal dopants and the amount of that transition metal present